Periodica Polytechnica
Mechanical Engineering

Three-dimensional Analysis of Air Flow in a Flat Plate Solar Collector

62(2), pp. 126-135, 2018
https://doi.org/10.3311/PPme.11255

Mohammed Amine Amraoui[1*], Khaled Aliane[2]

RESEARCH ARTICLE

Received 13 July 2017; accepted after revision 13 December 2017

Abstract

This paper presents the study of fluid flow and heat transfer in solar flat plate collector by using Computational Fluid Dynamics (CFD) which reduces time and cost. In the present paper the computational fluid dynamics (CFD) tool has been used to simulate the solar collector for better understanding the heat transfer capability. 3D model of the collector involving air inlet, the collector is modeled by ANSYS Workbench and the grid was created in ANSYS ICEM. The results were obtained by using ANSYS FLUENT and ANSYS CFX. The objective of this work is to compare theoretically and experimentally work done with the work done by using computational fluid dynamics (CFD) tool with respect to flow and temperature distribution inside the solar collector. The outlet temperature of air is compared with experimental results and there is a good agreement in between them.

Keywords

flat plate solar collector, fluid flow, k_ε turbulent model, CFD

[1] Department of Mechanical Engineering, Faculty of Technology,
University Djillali LIABES Sidi-Bel-Abbès,
BP 89 22000 Sidi-Bel-Abbès, Algeria

[2] Department of Mechanical Engineering, Faculty of Technology,
University Aboubakr Belkaid Tlemcen,
22, Street Abi Ayed Abdelkrim Fg Pasteur B.P 119 13000, Tlemcen, Algeria

[*] Corresponding author, e-mail: amraoui_mohammedamine@yahoo.fr

1 Introduction

Flat-plate collectors are the most common solar collector for solar water-heating systems in homes and solar space heating. A typical flat-plate collector is an insulated metal box with a glass or plastic cover (called the glazing) and a dark-colored absorber plate. These collectors heat liquid or air at temperatures less than 80°C.

Given the small heat exchange between the absorber plate and the caloporting fluid, techniques have been developed to improve to transfer.

O. Mahfoud et al. [1] presents a numerical simulation on air flow and heat transfer characteristics in solar air collectors mounted with obstacles. Computational Fluid Dynamics, 'CFD' based on the finite volume method, SIMPLE algorithm and the turbulence standard (k-ε) model have been implemented. A numerical 2D model of dynamic air vein solar collectors with 1400 mm length and 25 mm air gap was used to evaluate hydrodynamic and heat transfer phenomena of flow patterns in the annular passageways, precisely the heat transfer around 13 chicanes. The chicane is formed with two parts: the first is perpendicular to the air flow and the second is titled ($\alpha = 60°$), they are mounted in successive rows, oriented perpendicular to the air flow. It is apparent that the turbulence created by the chicanes resulting in greater increase in heat transfer over the air vein. The pressure drops are analyzed vs. the Reynolds number and shown good agreements with experimental and semi-empirical relationship results. The mass flow rates effect on the velocity magnitude is analyzed. It was found that the mass flow rate variation has a slight effect on velocity evolution.

Anil Singh Yadav et al. [2] presents the study of heat transfer in a rectangular duct of a solar air heater having.

Triangular rib roughness on the absorber plate by using Computational Fluid Dynamics (CFD). The effect of Reynolds number on Nusselt number was investigated. The computations based on the finite volume method with the SIMPLE algorithm have been conducted for the air flow in terms of Reynolds numbers ranging from 3000-18000. A commercial finite volume package ANSYS FLUENT 12.1 is used to

analyze and visualize the nature of the flow across the duct of a solar air heater. CFD simulation results were found to be in good agreement with experimental results and with the standard theoretical approaches. It has been found that the Nusselt number increases with increase in Reynolds number.

In the study by Satya Prakash Nayak [3] CFD software has been used to perform a numerical simulation for enhance turbulent heat transfer. A present CFD analysis of heat transfer and flow pattern with artificial roughness in the form of different types of ribs, heated wall of rectangular duct for turbulent flow with Reynolds number range (3000-15000) and p/e (5 to 20) has been carried out with k-ω turbulence model is selected by comparing the predictions of different turbulence models with experimental results available in various literature. This study evaluates reattachment point, heat transfer and fluid flow behavior in a rectangular duct with different roughened ribs mounted on one of the principal wall (solar plate) by computational fluid dynamics software (Fluent 6.3.26 Solver).The results are validated by comparing with existing experimental data. The analysis shows that peak in local heat transfer occurs at the point of reattachment of the separated flow as observed experimentally. The normalized friction factors in a square duct roughened with various-shaped ribs at the same pitch ratio (P/e =12). In the given Reynolds number range, the trapezoidal -shaped ribs have the highest friction loss; whereas, the trapezoidal-shaped ribs have the lowest pressure drop. Furthermore, the triangular-shaped ribs have slightly higher friction factor than that of square-shaped ribs. Based on the law of the wall similarity.

The study by Prashant Baredar et al. [4] evaluates heat transfer and fluid flow behavior in a rectangular duct with inverted U- type turbulator roughened ribs mounted on one of the principal wall (solar plate) by computational fluid dynamics software (Fluent 6.3.26 Solver). In this study CFD software has been used to perform a numerical simulation for enhance turbulent heat transfer. In this study, the Reynolds-Averaged Navier–Stokes analysis is used as a numerical technique and the k-ε turbulent model with near-wall treatment as a turbulent model. The results are validated by comparing with existing experimental datas. Provision of ribs completely obstructs the viscous sub-layer adjacent to the hot wall, which generates eddies/recirculation zones upstream and downstream, Eddies not only reduce the heat transfer but also increase the pressure drop. With opening the passage downstream the rib, intensity of eddies formation can be reduced. A thin inclined U- turbulator geometry with a passage underside could definitely prevent totally the formation of eddies and also the redevelopment of two boundary layers at the reattachment point in between two adjacent ribs. Value of the Nusselt number increases sharply at low Reynolds number and this becomes constant or increases very slightly in comparison to low Reynolds number; This also satisfied our aim of solar collector application at low Reynolds number.

One key problem of using solar energy is low heat exchange between the coolant and absorber of the solar collector. By cons, the introduction of baffle (obstacles).

Arranged in rows in the ducts of these systems greatly improves heat transfer. K. Aliane et al. [5] study the influence of roughness at the insulation to increase thermal exchanges within the collector. A numerical study using finite volume methods is made to study the dynamic and thermal behavior of the airflow in a solar collector plane with and without baffles with rectangular roughness. This part of simulation has shown that upstream portion of the first baffle (area 'A'), the low speeds for the two types of collectors studied. In addition, the level of roughness (for the case of collector with roughness), that is near zero speed. This is equivalent to the formation a thin layer of fluid trapped in these asperities. With roughness embedded in the collector, the speed is very important in the region 'D', 'E' and 'C', and compared with the case without roughness collector, where the speed is very low. Regarding the temperature fields, and for the case without roughness, the temperature becomes high immediately downstream of the second baffle. As against, for the case with roughness, temperatures are progressive and significant from the first baffle values.

For a given simulation of actual solar collector air plane and given the best result of the characteristics of the fluid, researchers from the simulation of 2D to 3D simulation.

The use of artificial roughness on a surface is an effective technique to enhance the rate of heat transfer to fluid flowing in a duct (Nikuradse [6], Nunner [7], Dipprey and Sabersky [8], Webb and Eckert [9], Han [10], Hosni et al. [11]). Roughness elements have been used to improve the convective heat transfer by creating turbulence in the flow. However, it would result in an increase in friction losses and hence, greater power requirement by fan or blower. In order to keep the friction losses at a minimum level, the turbulence must be created only in the region very close to the surface i.e. in laminar sub-layer. The surface roughness can be produced by several methods, such as sand blasting, machining, casting, forming, welding ribs and wires along the surface. Different types of wire, rib or wire mesh with different shapes, orientations and configurations on the surface are used to create required roughness. S.V. Karmare et al. [12] presents a study of fluid flow and heat transfer in a solar air heater by using Computational Fluid Dynamics (CFD) which reduces time and cost. In this analysis collector plate is made rough with metal ribs of circular, square and triangular cross-section, having 600 Inclination to the air flow. The grit rib elements are fixed on the surface in staggered manner to form defined grid. To validate CFD results, experimental investigations were carried out in the laboratory. The experimental results of the roughened solar air heater are compared with CFD analysis results. The square cross-section ribs with 580 angle of attack give maximum heat transfer. The percentage enhancement in the heat transfer for square plate over smooth surface is 30%.

The unglazed transpired solar air collector is now a well-recognized solar air heater for heating outside air directly, Chongjie Wang et al. [13] introduced numerical simulation tools into the solar air collector research area, analyzed the performance characteristics of the unglazed transpired solar air collector and compared them with several kinds of traditional solar air collectors. The results showed that the unglazed transpired solar air collector has unparalleled advantages in the ventilation preheating area and also proves that CFD tools have their own advantages in the solar air collector research area.

The prices of energy resources used for grain drying are increasing year by year. In order to reduce costs, research into methods of saving energy in grain drying is in progress in the Research Laboratory of Grain Drying and Storing of the Faculty of Engineering, the LUA. Equipment (J. Palabinskis, A. Aboltins, A. Lauva and N. Karpova-Sadigova) [14] for experimental research into the materials of solar collectors was built in the research laboratory for research purposes in 2005. The construction of the equipment allows for simultaneous comparative studies of two materials. The experimental data are metered and recorded in the electronic equipment REG. Cell polycarbonate PC (bronze, henceforth referred to as polycarbonate) with absorbers steel-tinplate and black-coloured wood was researched in comparison to the polyvinylchloride film (henceforth referred to as a film). The researches were made with different air velocities. The air heating degree ΔT in the solar collector is dependent on solar radiation I and air velocity v in the solar collector. In the experimental equipment, which is 1.5 meters in length, the air was heated to ΔT = 6°C at the velocity v = 0.5 m s-1. For theoretical investigation of the air heating power in solar systems the mathematical model is applied; the solution can be used for estimation of different materials /absorbents/ and their heat source.

Anup Kumar et al. [15] a study the behavior of solar air heater with and without porous media and also to compare their performance under different set of conditions, obtained by changing various governing parameters like air mass flow rate, inlet air temperature, spacing between top cover and absorber plate and intensity of solar radiation. The problems have been solved by the Finite Difference Method. They presented the mathematical model for predicting the heat transfer characteristics and the performance of solar air heater with and without porous media. The solar air heater with porous media gives higher thermal efficiency than without porous media. The thermal conductivity of porous media has significant effect on the thermal performance of the solar air heater. The work has been carried out on GAMBIT and FLUENT software as it is standard tool for flow analysis and widely acceptable. A double pass flat plate solar air heater model is prepared subjected to the relative loads and constraints and results are obtained for the proposed models.

From the various viewpoints encountered in the study of solar air collectors, Ben Slama Romdhane [16] concludes that the introduction of suitable baffles in solar air collectors increases the couple efficiency – increase in temperature. These baffles, placed in the air channel situated between the insulator and the absorber, have the particularity of extending the trajectory of the circulation, to keep the caloporting air constantly in contact with the absorber, and finally to play the role of wings and improving the heat transfer from the absorber to the caloporting air. So, solar air collectors can become as efficient as the solar water collectors and will have the same efficiency. The measurements showed that the efficiency reached 80% for the best type of chicanes, for an air flow rate of 50 $m^3/h/m^2$, and a temperature increase of 600°C.

The success of the solar energy applications is closely related to the performance of the collectors which convert it. For the collectors whose caloporting fluid is water; thermal transfer is made suitably because water is a good conductor of heat. However, for solar air collectors, heat transfer is low. In this paper, we show the design of air collector on which it is possible to act to improve the heat transfer between the absorber and the caloporting air and thus to favor the energetic efficiency while assuring a maximum increase of temperature. we will introduce of baffles by simulation We observe the formation of a meandering flow. In this case, it is clear that the length of the trajectory is more than double that of the collector, thus increasing the air speed and the heat transfer. On the other hand, the size of the dead zones is considerable.

2 Problematic

2.1 Geometry

The model of the solar collector has been studied experimentally by [17]. The air flow moves between the insulation and the absorber, with two types of baffles.

Baffles arranged transversely to the insulation 80% of each occupant collectors width (Fig. 1), a rectangular shape, and which have the same height as the passage, they are five in number arranged in a labyrinth.

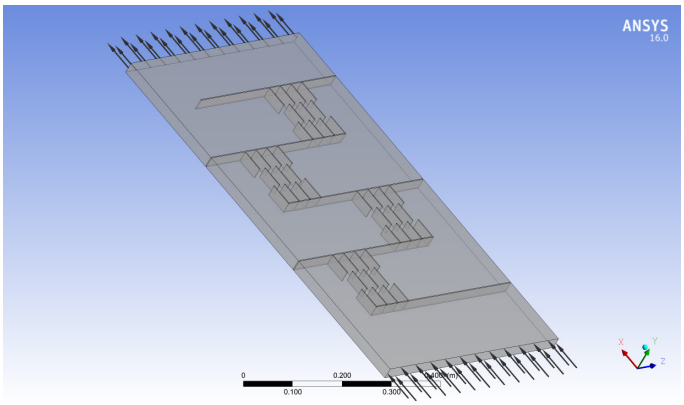

Fig. 1 Sketch for the solar collector

Baffles small size 50x25 mm, of rectangular shape, placed in the space between those of larger sizes, in other words in the compartments of the labyrinth.

The collector:

length (L)=900 mm.

width (l)=500 mm.

Height of the flow path=25 mm.

The baffles:

The space between the baffles forming the labyrinth=150 mm

The space between the baffles small=30 mm.

Height baffles=25 mm.

2.2 Governing equations

The Mass Conservation Equation:

The equation for conservation of mass, or continuity equation, can be written as follows:

$$\nabla.\left(\rho\vec{v}\right)=0. \tag{1}$$

Momentum Conservation Equations:

Conservation of momentum is described by

$$\nabla.\left(\rho\vec{v}\vec{v}\right)=-\nabla p+\nabla\left(\bar{\bar{\tau}}\right)+\rho\vec{g}. \tag{2}$$

$\rho\vec{g}$ is the gravitational body force.

The stress tensor $\bar{\bar{\tau}}$ is given by

$$\bar{\bar{\tau}}=\mu\left[\left(\nabla\vec{v}+\nabla\vec{v}^{T}\right)-\frac{2}{3}\nabla.\vec{v}I\right]. \tag{3}$$

The second term on the right hand side is the effect of volume dilation.

The Energy Equation:

$$\nabla.\left(\vec{v}\left(\rho E+p\right)\right)=\nabla.\left(k_{eff}.\nabla T-\sum_{j}h_{j}.\vec{j}_{j}+\left(\bar{\bar{\tau}}_{eff}.\vec{v}\right)\right). \tag{4}$$

The first three terms on the right-hand side of Eq. (4) represent energy transfer due to conduction, species diffusion, and viscous dissipation, respectively.

$$.k_{eff}=k+\frac{c_{p}\mu_{t}}{\mathrm{Pr}_{t}}. \tag{5}$$

The default value of the turbulent Prandtl number is 0.85.

$$E=h-\frac{p}{\rho}+\frac{v^{2}}{2}. \tag{6}$$

$$h=\sum_{j}Y_{j}h_{j}+\frac{p}{\rho}. \tag{7}$$

$$h_{j}=\int_{T_{ref}}^{T}c_{p.j}dT. \tag{8}$$

Where T_{ref} 298.15 K.

Transport Equations for the Standard k-ε Model:

The turbulent kinetic energy, k, and its turbulent eddy dissipation, ε, are obtained from the following transport equations:

$$\frac{\partial}{\partial x_{i}}\left(\rho ku_{i}\right)=\frac{\partial}{\partial x_{j}}\left[\left(\mu+\frac{\mu_{t}}{\sigma_{k}}\right)\frac{\partial k}{\partial x_{j}}\right]+G_{k}-\rho_{\varepsilon}. \tag{9}$$

And

$$\frac{\partial}{\partial x_{i}}\left(\rho\varepsilon u_{i}\right)=\frac{\partial}{\partial x_{j}}\left[\left(\mu+\frac{\mu_{t}}{\sigma_{\varepsilon}}\right)\frac{\partial\varepsilon}{\partial x_{j}}\right]+C_{1\varepsilon}\frac{\varepsilon}{k}G_{k}-C_{2\varepsilon}\rho\frac{\varepsilon^{2}}{K}. \tag{10}$$

Modeling the Turbulent Viscosity:

The turbulent (or eddy) viscosity, μ_{t}, is computed by combining k and ε as follows:

$$\mu_{t}=\rho.C_{\mu}\frac{k^{2}}{\varepsilon}. \tag{11}$$

Where C_{μ} is a constant.

Model Constants:

The model constants $C_{1\varepsilon}$, $C_{2\varepsilon}$, C_{μ}, σ_{k} and σ_{ε} have the following default values:

$C_{1\varepsilon}=1.44$, $C_{2\varepsilon}=1.92$, $C_{\mu}=0.99$, $\sigma_{k}=1.0$, $\sigma_{\varepsilon}=1.3$

2.3 Collector study

The heated fluid is here air flowing along the x axis. We designate by:

« ℓ »: the width of the flow (m).

« e »: the thickness (m).

« L »: the length (along x) (m).

If T_{1} is the inlet air temperature, T_{2} the outlet temperature, q_{v} the air flow, the solar flow is perpendicular to the collector; this flow is denoted by φ_{0} in W/m^{2} and if the outward thermal losses are neglected, the total power received by the sensor is entirely transmitted to the air:

$$\varphi_{0}.\ell.L=\rho.c_{p}.q_{v}\left(T_{2}-T_{1}\right) \tag{12}$$

ρ: average density of air ρ = 1.25 kg/m^{3}

c_{p}: average mass heat of air c_{p} =1000 j/kg °C

At abscissa x, the average fluid temperature is denoted by T and the temperature of the absorbent wall by T_{p}.

If we isolate an elemental air of length dx, we will obtain:

Power received by the collector:

$$\varphi_{0}.\ell.dx \tag{13}$$

Power carried by the fluid:

$$\rho.c_{p}.q_{v}.dT=h.\ell.dx\left(T_{p}-T\right) \tag{14}$$

T_{p} is the temperature of the absorbent wall where h is the transfer coefficient ($w/m^{2}°C$) between the absorbent wall and the fluid, it can be calculated by the definition relation:

$$\frac{h.dH}{\lambda}=Nu \tag{15}$$

Nu: Nusselt number of flow.

λ: Conductivity of the air (w/m°C)

dH: Hydraulic diameter of the section.

If “e” is much smaller than “ℓ”, the hydraulic diameter is substantially equal to 2e.

Lost power through insulation:

By conduction, we will have:

$$\frac{\lambda_i}{E_i}.\ell.dx\left(T_p - T_e\right) \tag{16}$$

λ_i: Conductivity of the insulation (w / (m °C)).

E_i: Thickness of the insulation (m).

T_e: Outside temperature (equal to T_1).

We will have a steady state:

$$\begin{aligned}\rho.c_p.q_v.dT &= \frac{\lambda.Nu}{2e}.\ell.dx\left(T_p - T\right)\\ &= \varphi_0.\ell.dx - \frac{\lambda_i}{E_i}.\ell.dx\left(T_p - T_e\right)\end{aligned} \tag{17}$$

By eliminating T_p between these equations, we will finally obtain the differential equation:

$$\frac{dT}{\varphi_0 + \frac{\lambda_i}{E_i}.\left(T_e - T\right)} = \frac{\ell.dx}{\rho.c_p.q_v\left(1 + \frac{\lambda_i}{E_i}.\frac{2e}{\lambda.Nu}\right)} \tag{18}$$

Let's integrate this relationship between entry and exit:

$$\int_{T_e}^{T_2}\frac{dT}{\varphi_0 + \frac{\lambda_i}{E_i}.\left(T_e - T\right)} = \int_0^L \frac{\ell.dx}{\rho.c_p.q_v\left(1 + \frac{\lambda_i}{E_i}.\frac{2e}{\lambda.Nu}\right)} \tag{19}$$

$$-\frac{E_i}{\lambda_i}\ln\left[\varphi_0 + \frac{\lambda_i}{E_i}.\left(T_e - T\right)\right]_{T_e}^{T_2} = \frac{\ell.L}{\rho.c_p.q_v\left(1 + \frac{\lambda_i}{E_i}.\frac{2e}{\lambda.Nu}\right)} \tag{20}$$

From where the value of the temperature T_2 at the exit of the collector:

$$T_2 = T_e + \varphi_0\frac{E_i}{\lambda_i}\left[1 - \exp\left(-\frac{\lambda_i}{E_i}.\frac{\ell.L}{\rho.c_p.q_v\left(1 + \frac{\lambda_i}{E_i}.\frac{2e}{\lambda.Nu}\right)}\right)\right] \tag{21}$$

$$\Delta T = \varphi_0\frac{E_i}{\lambda_i}\left[1 - \exp\left(-\frac{A}{1-B}\right)\right] \tag{22}$$

With

$$A = \frac{\lambda_i.\ell.L}{E_i.\rho.c_p.q_v}\ ,\ B = \frac{\lambda_i}{E_i}.\frac{2e}{\lambda.Nu}$$

When the insulation is perfect $\frac{\lambda_i}{E_i} \to 0$, and we fall back on the Eq. (12).

Collector performance study:

The output is defined by the ratio of the real power, on the power provided by the sun. We will have:

$$\eta = \frac{\rho.c_p.q_v\left(T_2 - T_1\right)}{\varphi_0.\ell.L} \tag{23}$$

$$\eta = \frac{\rho.c_p.q_v E_i}{\lambda_i.\ell.L}\left[1 - \exp\left(-\frac{\lambda_i}{E_i}.\frac{\ell.L}{\rho.c_p.q_v\left(1 + \frac{\lambda_i}{E_i}.\frac{2e}{\lambda.Nu}\right)}\right)\right] \tag{24}$$

Ask $1/A = \frac{\rho.c_p.q_v E_i}{\lambda_i.\ell.L}$

$$\eta = \frac{1}{A}\left[1 - \exp\left(-\frac{A}{1-B}\right)\right] \tag{25}$$

2.4 The boundary conditions

As the flow is turbulent, k–ε model is selected as turbulent model for further analysis of the problem. No slip condition is applied to all the 'walls'. According to the models selected earlier the equations which were going to be solved by continuity equation or energy equation or momentum equation or equation for turbulence.

To solve these equations, under-relaxation factors are used:

The velocity of the air at the inlet: $u_0 = 0.02216$ m/s corresponding for rate flow 79.79m³/hm².

The air temperature at the inlet Te = 300 K

The turbulent kinetic energy at inlet

$k = 0.005\ .U_0^2 = 2.456\cdot10^{-6}\ m^2/s^2$

The energy dissipation at inlet $\varepsilon = 0.1\cdot k^2 = 6.03\cdot10^{-13}\ m^2/s^3$

The temperature of the absorber: Tabs = 380 K

(corresponding to a solar flux value equal to 800 w/m²).

The temperature of the insulation and the lower baffle:

$T_{iso} = 340$ K

The outlet pressure: Ps = Patm.

2.5 Mesh

There was a need to place very fine mesh near the ribs to predict the results accurately see Fig. 2 and Fig. 3.

Meshing of the domain was done using ANSYS, with non-uniform quad grid of 1 mm grid size. This size was suitable to resolve the laminar sub-layer. A general practice is to use fine mesh size in the area where greater details are desired such as fins and coarse mesh in areas of small changes in domain geometry. Non uniform high density mesh in inter fin region and on edges and corners were employed while low density mesh was adapted in the smooth wall regions. The mesh density for the CFD analyses was kept at 51 x 34 x 2. This helped in economizing the number of cells needed for acceptable computational time and computer memory, Figs. 2 and 3 show the grid pattern for the flow domain.

3 Discussions and interpretations

The results obtained from the CFD analysis of solar flat plate collector are presented in this section. The simulation is carried out for different flow. Then the results obtained by this simulation compared with the experimental results as shown in

Table 1. It seems that the difference between experimental and simulated outlet temperature for different flow is almost 4˚C.

All dimensions are in centimeters as shown by Table 1.

Table 1 Comparison of experimental and cfd results

Flow m^3/hm^2	Collector temperature obtained by CFD (˚C)	Collector Temperature [17] (˚C)
Q1=79.79	53	50
Q2=76.32	53	50
Q3=74.01	54	51
Q4=69.96	54	52.3
Q5=64.76	59	56
Q6=58.97	62	58
Q7=42.79	65	63
Q8=37.58	65	63
Q9=23.71	69	68

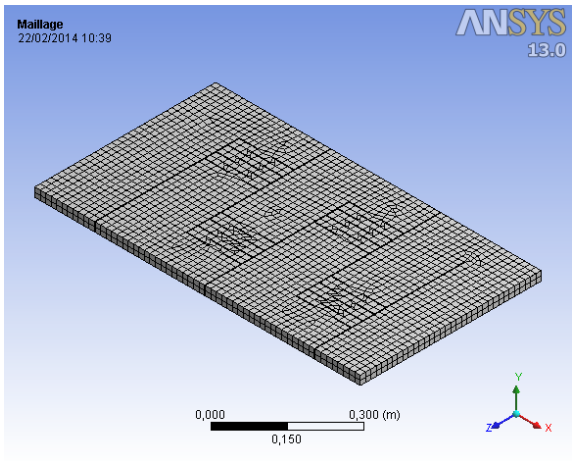

Fig. 2 3D mesh of Solar Flat Plate Collector

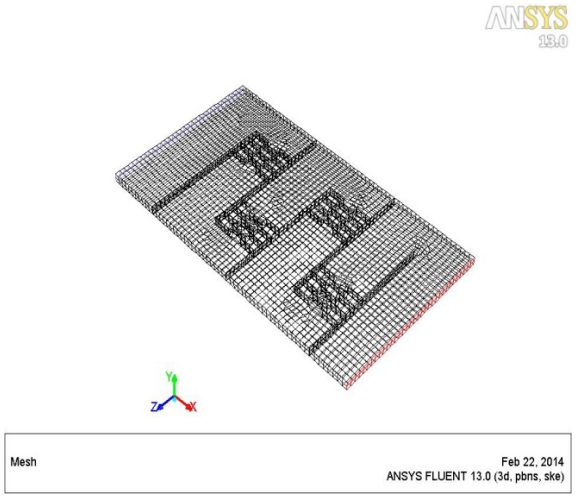

Fig. 3 Flow domain with Baffles arranged transversely and Baffles small

3.1 Temperatures Field

The temperature distribution is obtained by CFD simulation. The contour plots obtained for temperature distribution is given by Fig. 4.

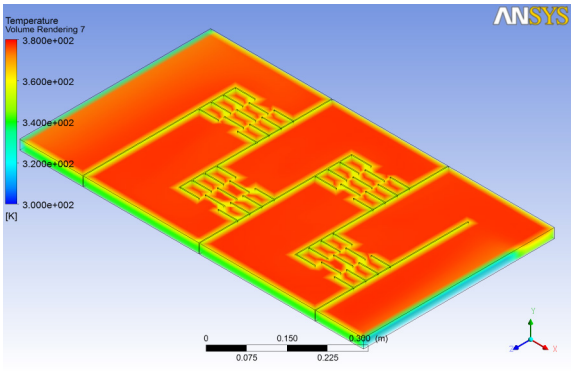

Fig. 4 Temperatures Field for the collector

As air passes above absorber the heat exchange takes place from the surface to air. The air very close to surface gets heated due to convection. This primary hot layer mixes with the secondary cold air due to baffles, and heat transfer takes place due to conduction and convection. As a result the temperature of air close to surface is higher, and goes on decreasing away from the surface up to one third height of the duct.

Fig. 5 shows the distribution of the temperature field for a cross section in the plane X, Z At the entrance, the air has a temperature of 300K, it begins to apply heat across half the distance between the inlet and the first transverse baffle it reaches a temperature of 335K, bypassing the latter, it reaches a temperature of about 350K. In conclusion follows that the flow of air keeps the same temperature (350 K), they cross the rows of baffles until exit.

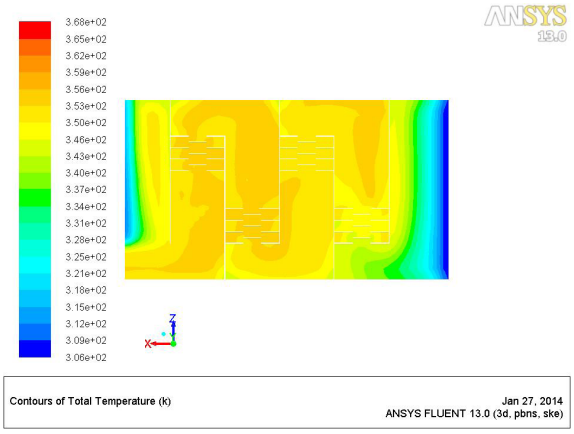

Fig. 5 Temperatures Field (plane X, Z)

3.2 The velocity vector V

In this case (Fig. 6), it is clear that the length of the trajectory is more than double that of the collector thanks baffles, thus increasing the air speed. On the other hand, the size of the dead zones is considerable.

To cure the problem of the large dead zones, let us introduce longitudinal baffles which will extend the flow and will reduce the extent of the dead zones to a minimum. The efficiency is very much increased.

Figs. 7, 8, 9, 10 and 11 shows the shape of the current lines around of different transverse baffles small baffles Fig.

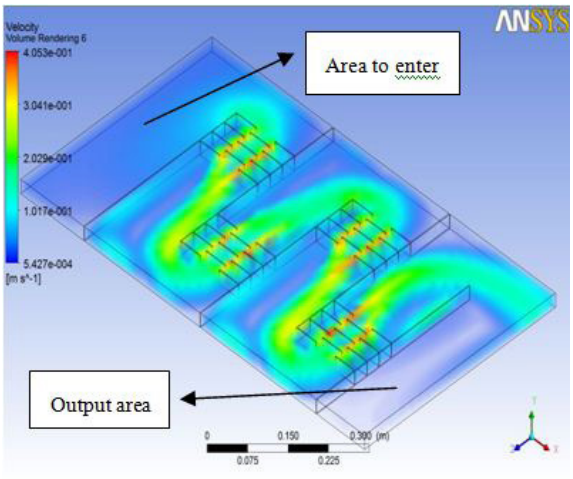

Fig. 6 Velocity distribution

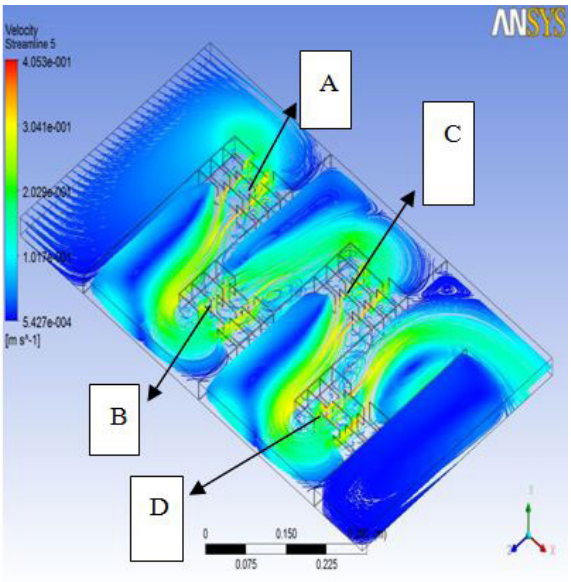

Fig. 7 Streamlines for velocity distribution

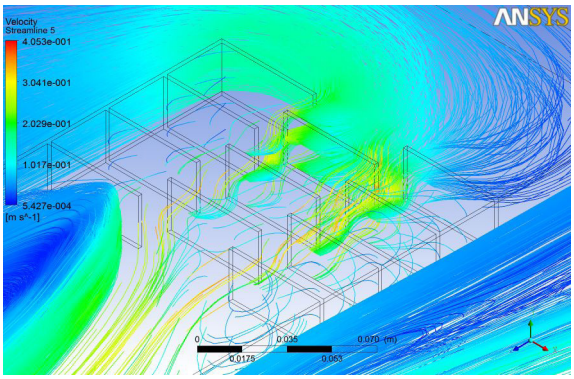

Fig. 8 Streamlines for velocity distribution (area A)

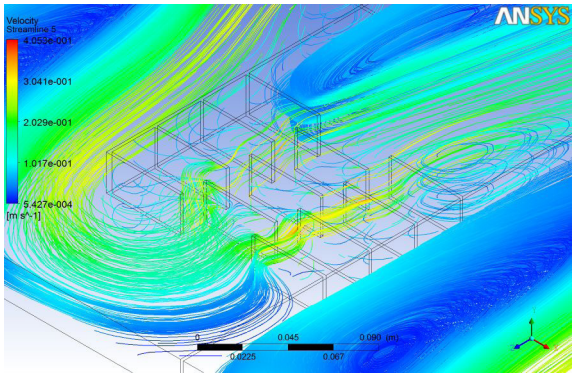

Fig. 9 Streamlines for velocity distribution (area B)

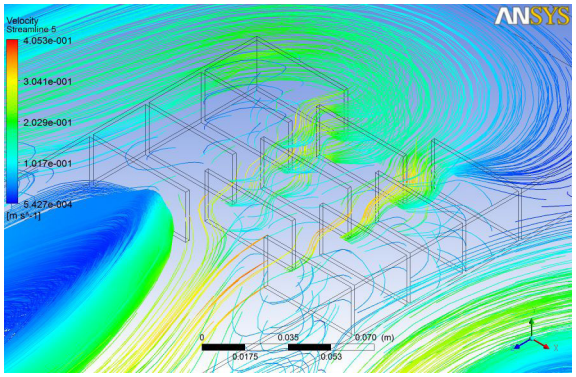

Fig. 10 Streamlines for velocity distribution (area C)

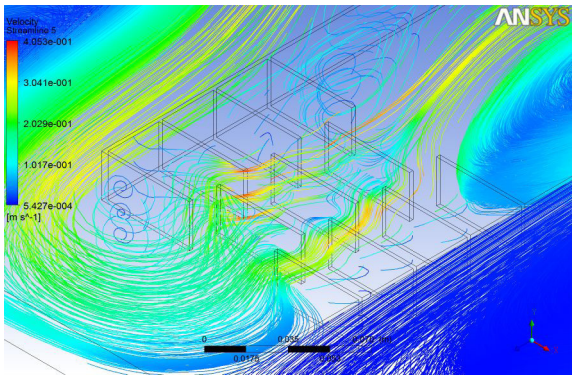

Fig. 11 Streamlines for velocity distribution (area D)

7 shows that the lines of current are accumulated around the small baffles which accelerates the flow in the place that the due to the narrowing of the flow section in this area. While transverse baffles promotes the appearance of an undesirable recirculation zone.

Figs. 8, 9, 10 and 11 write in detail the flow around this grouping baffles found just entered (area A), middle (area B and C) and the left collector (area D.) these figures show that the main flow is performed in the XZ plane: the flow bypasses the baffles in the middle as it passes over baffles which are integral with the transverse baffles.

3.3 The velocity components

Baffles small on the underside of the collector solar increase the velocity components.

The scope of the transverse velocity component in the main direction of flow and shown in Fig. 12. In remote areas of the baffles, the speed is weakened compared to five times the speed of air came through against, it increases more than ten times the speed of the input around small baffles: these speeds are positive (in the same direction of flow) for the first and

third group of small baffles (areas A, C) and it takes a negative value in the second and fourth group (areas B, D).

The velocity component v and guest Fig. 13. The Figure shows that this component of velocity is nearly zero following any of the surface collector (2.54 10^{-4}m/s) with the exception of the group will turn as small baffles shows the Figs. 8, 9, 10 and 11.

Fig. 14 shows the component of the velocity w, we find that this rate is very negligible in remote areas baffles (2.87 10^{-3}m/s) by cons it is very important to around the group of small baffles 0.39 m / s (twenty times the speed of input).

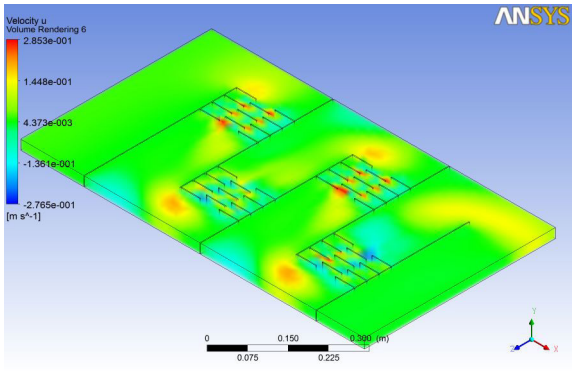

Fig. 12 The velocity component u

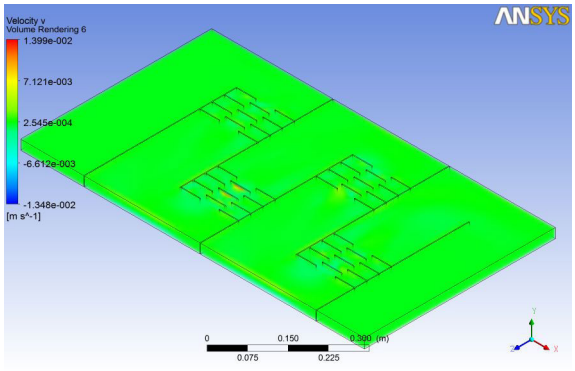

Fig. 13 The velocity component v

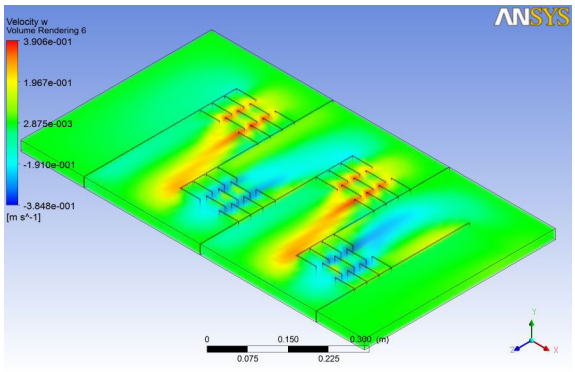

Fig. 14 The velocity component w

3.4 Turbulent kinetic energy (k)

The distribution of turbulent kinetic energy (k) is given by Fig. 15, it is clear that the flow has a turbulent kinetic energy throughout their trajectory. There is a considerable increase of turbulent kinetic energy in baffles small.

3.5 Turbulent eddy dissipation (ε)

Turbulent eddy dissipation (ε) is given in Fig. 16. This dissipation varies between 6.03.10^{-6} m^2/s^3 and 1.32.10^{-1} m^2/s^3. There is a significant dissipation over the vicinity of the small baffles.

3.6 Velocity Profiles

The velocity profiles are not similar, the velocity is very important for the profile of the output area, the velocity Reaches 0.032 m/s see Fig. 17.

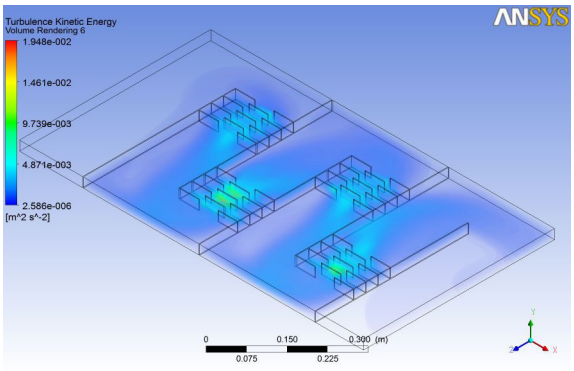

Fig. 15 Turbulent kinetic energy (k)

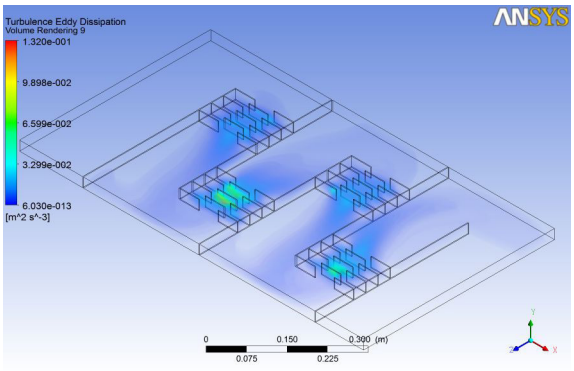

Fig. 16 Turbulent eddy dissipation (ε)

3.7 Turbulent kinetic energy (k) profiles

The different profiles are drawn between the insulation and the absorber.

The turbulent kinetic energy (k) is very important in output area to the position (0.01 to 0.015 m) Compared to area to enter see Fig. 18.

3.8 Turbulent eddy dissipation (ε) profiles

The turbulent eddy dissipation (ε) is very important in output area to the position (0.01 to 0.015 m) Compared to area enter see Fig. 19.

3.9 Temperatures profiles

The temperature is very important in output area Compared to area to enter see Fig. 20.

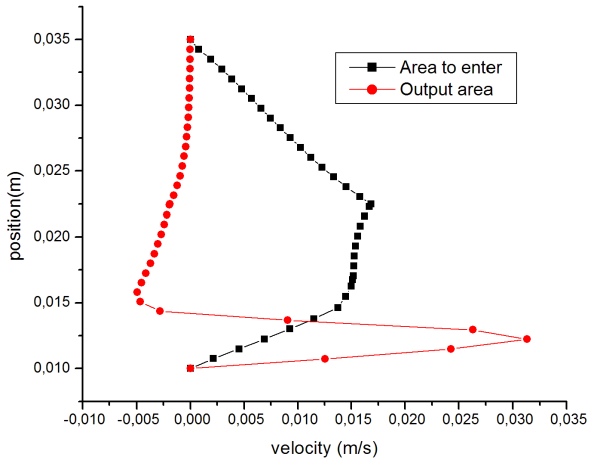

Fig. 17 Velocity profiles

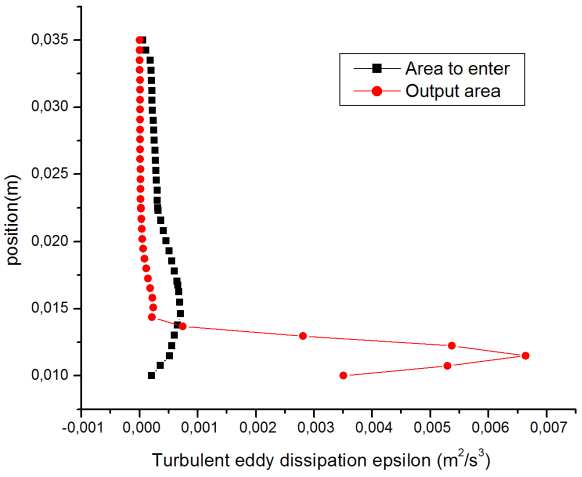

Fig. 19 Turbulent eddy dissipation (ε) profiles

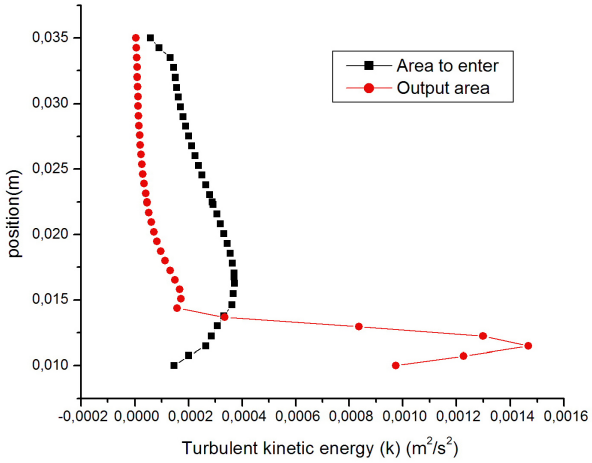

Fig. 18 Turbulent kinetic energy (k) profiles

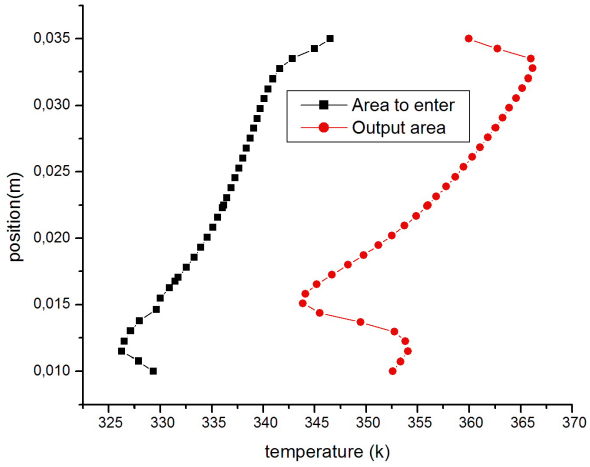

Fig. 20 Temperatures profiles

4 Conclusion

From the various viewpoints encountered in the study of solar air collectors, it becomes evident that the introduction of suitable baffles in solar air collectors increases the couple efficiency – increase in temperature. These baffles, placed in the air channel situated between the insulator and the absorber, have the particularity of extending the trajectory of the circulation, to keep the caloporting air constantly in contact with the absorber, and finally to play the role of wings and improving the heat transfer from the absorber to the caloporting air.

There is a good agreement between the experimental and simulated results for outlet air temperatures. Although there are some small discrepancies due to some experimental imperfectness matters, we still have a good confidence in the CFD simulation program that can be used in the future for more complex solar collector problem.

Nomenclature

c_p	Heat capacity at constant pressure, volume (J/kg.K).
$C_{1\varepsilon}$	Constants.
$C_{2\varepsilon}$	Constants.
C_μ	Constants.
E	The total energy (J).
$\vec{g}$	Gravitational acceleration (m/s^2).
G_k	The generation of turbulence kinetic energy due to the mean velocity gradients.
h	Sensible enthalpy (energy/mass).
I	The unit tensor.
$\vec{J}_j$	The diffusion flux of species j.
k	The thermal conductivity (W/m.K).
k	The turbulent kinetic energy (m^2 /s^2).
k_{eff}	The effective conductivity.
p	The static pressure (pa).
Pr_t	The turbulent Prandtl numbers.
T	Temperature (K).
u_i	Velocity magnitude (m/s).
$\vec{v}$	Overall velocity vector (m/s).
Y_j	The mass fraction of species j.
$\bar{\bar{\tau}}$	The stress tensor (described below) (pa)
μ	The molecular viscosity (Pa.s).
μ_t	The turbulent (or eddy) viscosity (Pa.s).
ε	The turbulent eddy dissipation (m^2/s^3).
σ_k, σ_ε	The turbulent Prandtl numbers for k and ε respectively.
ρ	Density (kg/m^3).

References

[1] Mahfoud, O., Zedayria, M., Moummi, A., Moummi, N. "Numerical 2D study of air flow controlled by active technique in solar air collector." *Revue des Energies Renouvelables*. 16(1), pp. 159-170, 2013.

[2] Yadav, A. S., Bhagoria, J. L. "A CFD Analysis of a Solar Air Heater Having Triangular Rib Roughness on the Absorber Plate." *International Journal of ChemTech Research*. 5(2), pp. 964-971. 2013.

[3] Nayak, S. P., Shukla, P., Ghodke, S. "CFD Analysis of Solar Flat Plate Collector Heat Transfer and Fluid Flow Analysis of Roughness Rib in Solar Air Heater Duct by Computational Fluid Dynamics (CFD) Simulation." *International Journal of Advanced Research in Science, Engineering and Technology*. 1(3), pp. 15-20. 2012.

[4] Baredar, P., Kumar, S., Giri, A. J., Kumar, J. "Heat transfer and fluid flow analysis of roughness ribin solar air heater duct by computational fluid dynamics (CFD)." *Current World Environment*. 5(2), pp. 279-285. 2010.

[5] Aliane, K., Amraoui, M. A. "Etude numérique d'un capteur solaire plan à air ayant une rugosité rectangulaire." (Numerical study of an air plane solar collector with a rectangular roughness.) *Revue des Energies Renouvelables*. 16(1), pp. 129-141. 2013. (in French)

[6] Nikuradse, J. "Heat transfer and pressure drop in rough tubes." NACA, Technical Memorandum-1292, 1950.

[7] Nunner, W. "Heat transfer and pressure drop in rough tubes." *VDI Forschungsheft*. 455, pp. 5–39. 1956.

[8] Dipprey, D. F., Sabersky, R. H. "Heat and momentum in smooth and rough tubes at various Prenatal numbers." *International Journal of Heat and Mass Transfer*. 6(5), pp. 329-332. 1963. https://doi.org/10.1016/0017-9310(63)90097-8

[9] Webb, R. L., Eckert, E. R. G. "Application of rough surfaces of heat exchanger design." *International Journal of Heat and Mass Transfer*. 15(9), pp. 1647-1658. 1972. https://doi.org/10.1016/0017-9310(72)90095-6

[10] Han, J. C. "Heat transfer and friction in a channel with two opposite rib roughened walls." *Journal of Heat Transfer*. 106, pp. 774-781. 1984. https://doi.org/10.1115/1.3246751

[11] Hosni, M. H., Coleman, H. W., Taylor, R. P. "Measurement and calculations of rough wall heat transfer in the turbulent boundary layer." *International Journal of Heat and Mass Transfer*. 34(4-5), pp. 1067-1082. 1991. https://doi.org/10.1016/0017-9310(91)90017-9

[12] Karmare, S. V., Tikekar, A. N. "Analysis of fluid flow and heat transfer in a rib grit roughened surface solar air heater using CFD." *Solar Energy*. 84, pp. 409–417. 2010. https://doi.org/10.1016/j.solener.2009.12.011

[13] Wang, C., Guan, Z., Zhao, X., Wang, D. "Numerical Simulation Study on Transpired Solar Air Collector." *Renewable Energy Resources and a Greener Future*. VIII-3-4, 2006.

[14] Palabinskis, J., Aboltins, A., Lauva, A., Karpova-Sadigova, N. "The comparative material investigations of solar collector." *Agronomy Research*. 6(Special issue), pp. 255-261. 2008.

[15] Kumar, A., Mishra, A. K. "A CFD Investigation and Pressure Correlation of Solar Air Heater." *International Journal of Mechanical Engineering and Technology (IJMET)*. 4(2), pp. 401-417. 2013.

[16] Romdhane, B. S. "The air solar collectors: Comparative study, introduction of baffles to favor the heat transfer." *Solar Energy*. 81(1), pp. 139-149. 2007. https://doi.org/10.1016/j.solener.2006.05.002

[17] Abdelhafid, M. "Etude globale et locale du rôle de la géométrie dans l'optimisation des capteurs solaires plans à air." (Global and Local Study of the role of geometry in optimizing solar air flat plate collectors.) Phd Thesis, Université de Valenciennes et du Hainaut Cambresis, France. 1994. (in French)